

Axion-electrodynamics: a quantum field calculation

Marc Beutter^{*}, Andreas Pargner[†], Thomas Schwetz[‡] and Elisa Todarello[§]

*Institut für Kernphysik, Karlsruhe Institute of Technology (KIT),
76021 Karlsruhe, Germany*

Abstract

An axion background field induces tiny oscillating electric and magnetic fields in an external static magnetic field. This signature is used to search for axion dark matter. We use standard quantum field theory techniques to obtain an expression for a transition amplitude, from which we identify the classical electromagnetic fields induced by the background axion field. We confirm previous results, that if the spatial size R of the applied static magnetic field is small compared to the axion Compton wavelength λ , the induced electric and magnetic fields are parametrically suppressed by the small numbers $(R/\lambda)^2$ and R/λ , respectively, relative to the case when R is larger than λ . Our approach allows an intuitive interpretation in terms of 4-momentum conservation and momentum exchange via the photon propagator.

^{*}marc.beutter@student.kit.edu

[†]andreas.pargner@kit.edu

[‡]schwetz@kit.edu

[§]elisa.todarello@kit.edu

1 Introduction

The QCD axion [1, 2] is one of the most attractive candidates for the dark matter (DM) in the Universe. As noted by Sikivie [3], its coupling to the photon field via the anomaly term offers experimental avenues to search for galactic DM axions. A recent review about the flourishing field of axion haloscopes can be found in Ref. [4]. The traditional way to search for axion DM is axion–photon conversion in a resonant cavity, for example by the ADMX [5], HAYSTAC [6] or CULTASK [7] collaborations. These experiments explore the most favored mass region for QCD axion DM, around $10^{-6} - 10^{-5}$ eV. Slightly larger masses can be reached by dielectric haloscopes, such as MADMAX [8].

More recently, some ideas to explore the region of axion masses below 10^{-6} eV have been developed, see for instance Refs. [9, 10] and the ABRACADABRA [11], BEAST [12], DM Radio [13] or KLASH [14] projects. These searches are motivated in the context of more general axion-like particle (ALP) DM scenarios. While for the QCD axion both the axion mass m_a and the axion–photon coupling $g_{a\gamma}$ are related to the same fundamental scale (the breaking scale of the Peccei–Quinn symmetry [15, 16]), this needs not be the case in general. For ALPs, m_a and $g_{a\gamma}$ can be treated as independent parameters. This is the approach we take here, and we use the term “axion” in the more general sense, including also ALPs.

The axion–photon interaction is described by the Lagrangian

$$\mathcal{L}_{a\gamma} = -\frac{g_{a\gamma}}{4} a F_{\mu\nu} \tilde{F}^{\mu\nu} = g_{a\gamma} a \vec{E} \cdot \vec{B}. \quad (1.1)$$

Here, a denotes the axion field, $F_{\mu\nu} = \partial_\mu A_\nu - \partial_\nu A_\mu$ is the photon field-strength tensor and $\tilde{F}^{\mu\nu} = \frac{1}{2} \epsilon^{\mu\nu\rho\sigma} F_{\rho\sigma}$ its dual. The coupling constant $g_{a\gamma}$ has dimension 1/energy. In the presence of this term, the inhomogenous Maxwell equations are modified as [3, 9]

$$\vec{\nabla} \cdot \vec{E} = \rho_e - g_{a\gamma} \vec{B} \cdot \vec{\nabla} a \quad (1.2)$$

$$\vec{\nabla} \times \vec{B} - \frac{\partial \vec{E}}{\partial t} = \vec{j}_e - g_{a\gamma} \left(\vec{E} \times \vec{\nabla} a - \vec{B} \frac{\partial a}{\partial t} \right), \quad (1.3)$$

where ρ_e and \vec{j}_e are the external charge and current density, and we have used Lorentz–Heaviside units with $c = 1$.

Let us neglect axion-gradient terms and ignore the backreaction on the axion field, which we treat as a classical source. Then the background axion field in a homogeneous external magnetic field \vec{B}^{ext} induces an electric field,

$$\vec{E}^{\text{ind}} = -g_{a\gamma} a \vec{B}^{\text{ext}}. \quad (1.4)$$

The basic approach of Refs. [5–13] and similar proposals is to search for those tiny induced electric or magnetic fields, either by using broadband or resonant detection methods. Note that “tiny” means that, for a DM axion with $m_a \sim 10^{-5}$ eV and a coupling $g_{a\gamma} \sim 10^{-15}$ GeV $^{-1}$, a 7 T magnetic field induces an E field with a magnitude of the order 10^{-13} V/m.

Recently, there has been some controversy about the magnitude of the induced electromagnetic (EM) fields in the case of an inhomogeneous external magnetic field, more precisely, when the scale of inhomogeneity is comparable to or smaller than the Compton wavelength of the axion,

$$\lambda = \frac{2\pi\hbar}{m_a c} \approx 12 \text{ m} \frac{10^{-7} \text{ eV}}{m_a c^2}. \quad (1.5)$$

Considering typical sizes of axion detection experiments, we see that this question becomes relevant for $m_a c^2 \lesssim 10^{-6}$ eV. As discussed recently by Ouellet and Bogorad [17] and Kim et al. [18], for experiments small compared to λ the induced electric field from eq. (1.4) is suppressed by the small number $(R/\lambda)^2$, where R is the characteristic size of the external B -field used by the experiment. This result emerges when the appropriate boundary conditions are imposed on the solution of Maxwell’s equations. Tobar et al. [19] come to a different conclusion, referring to a quantum field theory calculation by Hong and Kim [20].

In the following, we will add to this discussion by performing a calculation of the axion-induced EM fields using quantum field theory methods, similar to those used by Hong and Kim [20]. By properly taking into account the spatial extension of the external B field via its Fourier transform, we obtain an intuitive understanding of the three cases of “large”, “small”, and “resonant” experiments, characterized by $R \gg \lambda$, $R \ll \lambda$, and $R \sim \lambda$, respectively, in terms of the available momentum transfer. Our calculation confirms the results of Refs. [17, 18]. Similar methods have been used by Hill [21, 22] to calculate an induced oscillating electric dipole moment of the electron and by Ioannisian et al. [23] in the context of dielectric haloscopes.

Let us clarify the notion of Compton wavelength in this context. In the situation of interest, namely detection of axion cold dark matter, we assume that the axion can be treated as a classical background field which oscillates with the frequency $\omega \approx m_a c^2/\hbar$. In a static external magnetic field, this corresponds to a source for the induced EM field, which oscillates with the frequency ω . Therefore the induced EM radiation has a wavelength $\lambda_{\text{EM}} = 2\pi c/\omega \approx \lambda$. It is the wavelength of this induced EM wave, which ultimately is responsible for setting the relevant length scale to be compared with R . For a zero velocity axion field, it coincides with the quantum mechanical Compton wavelength of an axion particle. In the following we will continue to use the term axion Compton wavelength λ to denote this length scale, keeping in mind however, that the axion is a classical field. From now on we will use natural units with $c = \hbar = 1$, such that $2\pi/\lambda = m_a \approx \omega$, where the interpretation of m_a as classical frequency is implied.

The outline of the paper is as follows. In section 2, we calculate the induced fields using standard quantum field theory methods to evaluate the relevant Feynman diagram. We discuss the effect of gradient terms, and show that in the limit of a homogeneous axion field, we recover the results of Refs. [17, 18], which were obtained by solving the classical Maxwell’s equations to leading order in $g_{a\gamma}$ and imposing the relevant boundary conditions. In section 3, we provide an explicit example by applying our method to the case of an

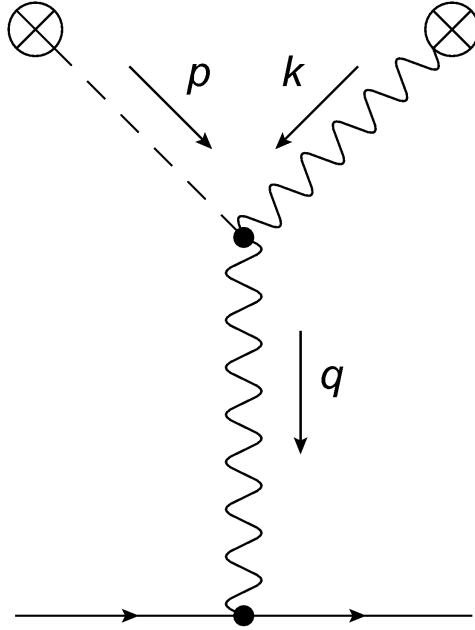


Figure 1: Interaction of an electron with an external EM field and the axion DM field (dashed line) via virtual photon exchange. The \otimes symbols indicate that the axion and the external EM field are treated as classical sources and are not affected by any backreaction.

infinitely long solenoid. Section 4 contains a discussion of our findings and the conclusions. In appendix A we derive the relation between the interaction Lagrangian and Hamiltonian densities for the axion–photon coupling, and in appendix B we give technical details on the calculations of section 3.

To fix the notation, greek indices take values 0,1,2,3, and roman ones denote only the spatial components 1,2,3. For a four-vector we write $(x^\mu) = (x^0, x^i) = (x^0, \vec{x})$, and our convention for the Minkowski metric is $(g_{\mu\nu}) = \text{diag}(1, -1, -1, -1)$.

2 Deriving the induced EM field

Let us first consider the interaction of a fermion, say an electron, with an external EM field:

$$\mathcal{L}_{\text{em}}(x) = -e\bar{\psi}(x)\gamma^\mu\psi(x)A_\mu^{\text{ext}}(x). \quad (2.1)$$

The transition amplitude for electron states $|i\rangle \rightarrow |f\rangle$ in first order in perturbation theory is

$$\mathcal{A} = -i\langle f| \int d^4x \mathcal{H}_I(x) |i\rangle = -i \int d^4x J^\mu(x) A_\mu^{\text{ext}}(x), \quad (2.2)$$

where the interaction Hamiltonian is given by $\mathcal{H}_I = -\mathcal{L}_{\text{em}}$ and we have defined $J^\mu \equiv e\langle f|\bar{\psi}\gamma^\mu\psi|i\rangle$. Combined with the free electron Hamiltonian, eq. (2.2) describes how an electron reacts to an external EM field.

Now we use a similar approach to calculate the effect of an external EM field in combination with the axion dark matter background field on an electron, based on the Feynman diagram in fig. 1. The relevant interaction Lagrangian is $\mathcal{L}_I = \mathcal{L}_{\text{em}} + \mathcal{L}_{a\gamma}$, with the axion–photon interaction given in eq. (1.1). It can be shown that the interaction Hamiltonian density can be written as $\mathcal{H}_I = -\mathcal{L}_I$ up to total derivatives, despite the derivative coupling of the photon, see appendix A. The transition amplitude $|i\rangle \rightarrow |f\rangle$, given the external axion and photon fields, can be calculated in second order in perturbation theory:

$$\mathcal{A} = \frac{(-i)^2}{2!} \langle f|T \int d^4x \int d^4y \mathcal{H}_I(x) \mathcal{H}_I(y)|i\rangle, \quad (2.3)$$

with T denoting the time-ordered product.

We use $aF_{\mu\nu}\tilde{F}^{\mu\nu} = 2a(\partial_\mu A_\nu)\tilde{F}^{\mu\nu} = -2(\partial_\mu a)A_\nu\tilde{F}^{\mu\nu} + \text{total derivative}$. Then we contract A_ν with the photon field coupled to the fermion current through the propagator. The other photon field as well as the axion are treated as external sources. The amplitude corresponding to the diagram in fig. 1 can be written as

$$\mathcal{A} = -i \int d^4x J^\mu(x) A_\mu^{\text{ind}}(x), \quad (2.4)$$

where (including a combinatorial factor 2)

$$A_\mu^{\text{ind}}(x) = ig_{a\gamma} \int d^4y D_{\mu\nu}(x-y) \partial_\rho a(y) \tilde{F}^{\rho\nu}(y). \quad (2.5)$$

The photon propagator in the Feynman gauge is given by

$$D_{\mu\nu}(x-y) = \int \frac{d^4q}{(2\pi)^4} \frac{-ig_{\mu\nu}}{q^2 + i\epsilon} e^{-iq(x-y)}. \quad (2.6)$$

We checked that physical quantities do not depend on the gauge choice—as it should be, see also Ref. [22]. By comparing eq. (2.4) with eq. (2.2), we see that the combination defined in eq. (2.5) acts just as an external EM field. Therefore we consider A_μ^{ind} as given in eq. (2.5) as the induced vector potential seen by the electron.

Let us now specify the properties of the external fields. For the external EM fields we assume that \vec{E} as well as \vec{B} are constant in time. This implies for the Fourier transform of the field strength tensor

$$\tilde{F}^{\rho\nu}(y) = \int \frac{d^3k}{(2\pi)^3} \tilde{F}^{\rho\nu}(\vec{k}) e^{i\vec{k}\cdot\vec{y}}. \quad (2.7)$$

Furthermore, we require that the external EM fields fulfill the full set of zeroth-order Maxwell’s equations (without the axion term).

Galactic DM axions can be described as classical wave packets:

$$a(y) = a_0 \int \frac{d^3p}{(2\pi)^3} a(\vec{p}) e^{-ip_y} \quad (2.8)$$

with $p^\mu = (\omega, \vec{p})$. Since a is a real field, it is understood that we should take the real part of eq. (2.8) as well as the following expressions. Using that axions are non-relativistic, we have $\omega \approx m_a + \vec{p}^2/2m_a$. The group velocity of an axion wave packet is $v^i = d\omega/dp^i = p^i/m_a$. The complex coefficients $a(\vec{p})$ can be interpreted in terms of a coarse-grained velocity distribution $f(\vec{v})$ by $|a(\vec{p})|^2 \propto f(\vec{v})$, see for example Ref. [24]. For galactic DM, the speed distribution is peaked at $|\vec{v}| \sim 10^{-3}$ with a typical spread of similar size, $\sigma_v \sim 10^{-3}$. We adopt the normalization $\int d^3p/(2\pi)^3 |a(\vec{p})|^2 = 1$ and fix the constant a_0 by assuming that the axion field provides the local dark matter density:

$$\rho_a \approx \frac{1}{2} m_a^2 a_0^2 \approx 0.4 \text{ GeV/cm}^3. \quad (2.9)$$

Now we plug eqs. (2.6) to (2.8) into eq. (2.5). The d^4y integration gives 4-momentum conservation via $(2\pi)^4 \delta(q^0 - p^0) \delta^{(3)}(\vec{k} + \vec{p} - \vec{q})$. After shifting the integration variable $\vec{q} \rightarrow \vec{q} + \vec{p}$ we obtain

$$A_\mu^{\text{ind}}(x) = -i g_{a\gamma} a_0 \int \frac{d^3q}{(2\pi)^3} \frac{d^3p}{(2\pi)^3} \tilde{F}_{\nu\mu}(\vec{q}) a(\vec{p}) \frac{p^\nu e^{i\vec{q}\cdot\vec{x}} e^{-ipx}}{m_a^2 - \vec{q}^2 - 2\vec{q}\cdot\vec{p} + i\epsilon}. \quad (2.10)$$

Note that this field is a classical object. In our derivation we start from a relativistic covariant Lagrangian to construct a quantum mechanical transition amplitude, eq. (2.3), using standard quantum field theory ingredients, in particular the Feynman propagator, eq. (2.6). However, in the comparison of our expression for the amplitude with eq. (2.2) it is clear that A_μ^{ind} in eq. (2.10) is a classical field. This is expected, since both the axion background field and the external EM fields are classical sources.

2.1 Discussion of the induced potential

The expression eq. (2.10) relates the induced field to the Fourier transform of the external EM field, showing how the induced field depends on the geometry of the external field. Our approach allows a physical interpretation in terms of the momentum transfer. In particular, we identify the following three cases.

- *Large experiment:* If the size of the experiment, i.e. the region of non-zero external field, is large compared to $1/m_a$, the Fourier transform $\tilde{F}_{\mu\nu}(\vec{q})$ is non-zero only for momenta $|\vec{q}| \ll m_a$. Hence, we can neglect all \vec{q} dependent terms in the denominator. This corresponds to the “contact interaction” with $q^2 \approx m_a^2$, as adopted in Ref. [20]. In this limit we will recover the results obtained there.
- *Small experiment:* The Fourier transform of the applied field extends to momenta much larger than m_a . The q -integral is dominated by the largest momenta and we can neglect $m_a^2 - 2\vec{p}\cdot\vec{q}$ compared to \vec{q}^2 in the denominator. As we will show below, in this limit the potential will be suppressed by a factor $(m_a R)^2$.
- *Resonant experiment:* If the size of the experiment is tuned to the Compton wavelength of the axion, the q integral will be dominated by momenta $|\vec{q}| \sim m_a$. We clearly see the

resonant enhancement in eq. (2.10). In this case the precise shape of the applied EM field around momenta of order m_a becomes important. Whether actually a resonance happens depends on additional boundary conditions. We will come back to this issue in section 4.

We can write the induced potential, eq. (2.10) in terms of the external E and B fields:

$$A_0^{\text{ind}}(x) = ig_{a\gamma}a_0 \int \frac{d^3q}{(2\pi)^3} \frac{d^3p}{(2\pi)^3} a(\vec{p}) \frac{e^{-i\omega t} e^{i(\vec{q}+\vec{p})\cdot\vec{x}}}{m_a^2 - \vec{q}^2 - 2\vec{q}\cdot\vec{p} + i\epsilon} \vec{p}\cdot\vec{B}^{\text{ext}}(\vec{q}) \quad (2.11)$$

$$\vec{A}^{\text{ind}}(x) = ig_{a\gamma}a_0 \int \frac{d^3q}{(2\pi)^3} \frac{d^3p}{(2\pi)^3} a(\vec{p}) \frac{e^{-i\omega t} e^{i(\vec{q}+\vec{p})\cdot\vec{x}}}{m_a^2 - \vec{q}^2 - 2\vec{q}\cdot\vec{p} + i\epsilon} \left[\omega\vec{B}^{\text{ext}}(\vec{q}) + \vec{p}\times\vec{E}^{\text{ext}}(\vec{q}) \right] \quad (2.12)$$

with $t \equiv x^0$. In the last factors in these expressions, we recognize the terms proportional to $g_{a\gamma}$ in the modified Maxwell's equations, eqs. (1.2) and (1.3). We recover the well known result, that an external static electric field couples to the axion only via gradient terms. The behaviour in the limits $\lambda \ll R$ or $\lambda \gg R$ is the same for the terms proportional to ω and \vec{p} . Therefore the above mentioned suppression for small experiments applies as well to momentum-dependent terms (here we disagree with a corresponding remark in Ref. [17]).

Let us briefly discuss the impact of the axion velocity distribution. Taking into account that the factor $a(\vec{p})$ confines the d^3p integral to the range $|\vec{p}| \sim 10^{-3}m_a$, we observe that in the cases of large and small experiment the d^3p integral factorizes and the induced field becomes proportional to

$$a_0 \int \frac{d^3p}{(2\pi)^3} p^\mu a(\vec{p}) e^{-ipx} = i\partial^\mu a(x). \quad (2.13)$$

Note that the induced potential is sensitive to the phases of $a(\vec{p})$, and therefore coherence effects may be relevant. A discussion of those is beyond the scope of this work.

In contrast, for the resonant case, details of the axion velocity distribution become relevant. Let us consider the p^0 -term and assume that $\tilde{F}_{\mu\nu}(\vec{q})$ has such a shape that the resonance dominates. Then we have approximately

$$A_\mu^{\text{ind}}(x)|_{\text{res.}} \approx ig_{a\gamma}a_0 \int_{|\vec{q}|\simeq m} \frac{d^3q}{(2\pi)^3} \tilde{F}_{0\mu}(\vec{q}) e^{i\vec{q}\cdot\vec{x}} \int \frac{d^3p}{(2\pi)^3} \frac{a(\vec{p})}{2|\vec{p}|\cos\theta - i\epsilon} e^{-ipx}, \quad (2.14)$$

where θ is the angle between \vec{p} and \vec{q} . We see that the finite momentum spread of the axions smears out the resonance. This is a manifestation of the well known result that the axion velocity spread leads to a quality factor of the resonance of order $1/v^2 \sim 10^6$. We see that the result depends sensitively on the shapes of $a(\vec{p})$ and $\tilde{F}_{\mu\nu}(\vec{q})$. Hence, in principle an experiment whose size is comparable to the Compton wavelength of the axion is sensitive to details of the local axion velocity distribution, in addition to phase-coherence effects, see Refs. [24, 25].

2.2 Zero-velocity axions

Let us from now on simplify the discussion by working in the approximation of axions with zero velocity, $\vec{p} = 0$ and $\omega = m_a$. In this limit the axion field becomes $a(x) = a_0 e^{-im_a t}$. Then, the time component of the potential vanishes, $A_0^{\text{ind}} = 0$. Using eq. (2.12), we find for the induced electric and magnetic fields

$$\vec{E}^{\text{ind}}(x) = -\frac{\partial \vec{A}^{\text{ind}}}{\partial t} = -g_{a\gamma} a_0 m_a^2 e^{-im_a t} \int \frac{d^3 q}{(2\pi)^3} \frac{e^{i\vec{q}\cdot\vec{x}}}{m_a^2 - \vec{q}^2 + i\epsilon} \vec{B}^{\text{ext}}(\vec{q}), \quad (2.15)$$

$$\vec{B}^{\text{ind}}(x) = \vec{\nabla} \times \vec{A}^{\text{ind}} = -g_{a\gamma} a_0 m_a e^{-im_a t} \int \frac{d^3 q}{(2\pi)^3} \frac{e^{i\vec{q}\cdot\vec{x}}}{m_a^2 - \vec{q}^2 + i\epsilon} \vec{q} \times \vec{B}^{\text{ext}}(\vec{q}). \quad (2.16)$$

We can use eqs. (2.15) and (2.16) to come back to the discussion of the limiting cases in which the size of the experiment is either large or small compared to the Compton wavelength of the axion. We assume that the external magnetic field is contained mostly in a volume of size R . This implies that the contribution to the momentum integral will be dominated by momenta $|\vec{q}| \lesssim 1/R$. As mentioned above, for the large experiment we can neglect \vec{q}^2 compared to m_a^2 in the denominator. This corresponds to a point-like interaction and we recover the “naive” result for the electric field, eq. (1.4), in agreement with Ref. [20].

In the case of a small experiment, the integral has to be evaluated including the pole. In order to get an estimate, we approximate the magnetic field by a top-hat in momentum space, $\vec{B}^{\text{ext}}(\vec{q}) \sim R^3 \vec{B}_0 \Theta(1/R - |\vec{q}|)$, with \vec{B}_0 having the dimensions of a magnetic field. Let us further consider the region in the center of the experiment $|\vec{x}| \ll R$, which implies $|\vec{q}\cdot\vec{x}| \ll 1$. In this limit we obtain¹

$$\vec{E}^{\text{ind}}(x) \simeq -g_{a\gamma} a_0 \vec{B}_0 e^{-im_a t} (R m_a)^2. \quad (2.17)$$

We see that the induced electric field is suppressed by the small number $(R/\lambda)^2$. Hence, our quantum field theory calculation confirms the behaviour in the large and small wavelength limits obtained in Refs. [17, 18] by solving the classical Maxwell’s equations. In section 3, we demonstrate for a specific field configuration that both approaches give quantitatively identical results.

Before that, we can provide a further consistency check. Let us start from eq. (2.15) and plug in the inverse Fourier transform for \vec{B}^{ext} . Then the $d^3 q$ integral can be performed, yielding

$$\vec{E}^{\text{ind}}(x) = g_{a\gamma} a_0 m_a^2 e^{-im_a t} \frac{1}{4\pi} \int d^3 y \frac{e^{im_a |\vec{x}-\vec{y}|}}{|\vec{x}-\vec{y}|} \vec{B}^{\text{ext}}(\vec{y}). \quad (2.18)$$

¹The integral can be evaluated by dividing it into a part up to momenta ϵ below the pole and from ϵ above the pole and taking the limit $\epsilon \rightarrow 0$:

$$\int_0^Q dq \frac{q^2}{m^2 - q^2} = -Q + \frac{m}{2} \log \frac{Q+m}{Q-m} \approx -Q,$$

where $Q \equiv 1/R > m$ and the last approximation holds for $Q \gg m$.

Using further that the external B -field is generated by a current \vec{j}_e with $\vec{\nabla} \times \vec{B}^{\text{ext}} = \vec{j}_e$ one can rewrite this expression as²

$$\vec{E}^{\text{ind}}(x) = g_{a\gamma} a_0 e^{-im_a t} \frac{1}{4\pi} \int d^3y \frac{e^{im_a |\vec{x}-\vec{y}|} - 1}{|\vec{x}-\vec{y}|} \vec{\nabla} \times \vec{j}_e(\vec{y}). \quad (2.19)$$

Similarly, in eq. (2.16) we can directly use $\vec{\nabla} \times \vec{B}^{\text{ext}} = \vec{j}_e$ to obtain

$$\vec{B}^{\text{ind}}(x) = -ig_{a\gamma} a_0 m_a e^{-im_a t} \frac{1}{4\pi} \int d^3y \frac{e^{im_a |\vec{x}-\vec{y}|}}{|\vec{x}-\vec{y}|} \vec{j}_e(\vec{y}). \quad (2.20)$$

Equations (2.19) and (2.20) agree with corresponding expressions in Ref. [17] (up to a missing factor $1/4\pi$). There, they have been derived as solutions of the Maxwell's equations with the method of retarded Green's functions, confirming the equivalence of the two methods. In this form we can also make direct contact with standard EM radiation theory, see e.g., Chapter 9 of Jackson [26]. We see that the limit of small experiment is equivalent to the near-field approximation, amounting to setting $e^{im_a |\vec{x}-\vec{y}|} \approx 1$ in integrals similar to the ones in eqs. (2.18) to (2.20), see also Ref. [17].

3 Infinitely long solenoid

In this section, we consider the case of an external magnetic field generated by a solenoid infinitely long in the z -direction and with radius R . In this setup, we use our method to calculate axion-induced EM fields. In cylindrical coordinates, the external magnetic field reads

$$\vec{B}^{\text{ext}}(\vec{x}, t) = B_0 \theta(R - r) \hat{e}_z. \quad (3.1)$$

Starting from eq. (2.12) in the limit of zero momentum axions, we obtain

$$A_{\text{ind}}^z(r, z, t) = ig_{a\gamma} a_0 B_0 e^{-im_a t} m_a R \int_0^\infty dq \frac{1}{m_a^2 - q^2 + i\epsilon} J_1(qR) J_0(qr), \quad (3.2)$$

where $J_n(x)$ is the Bessel function of the first kind of order n . The integral can be solved analytically (see appendix B for details):

$$A_{\text{ind}}^z(r, z, t) = ig_{a\gamma} a_0 B_0 e^{-im_a t} m_a R^2 \begin{cases} \frac{1}{m_a^2 R^2} - \frac{i\pi}{2} \frac{H_1^+(m_a R) J_0(m_a r)}{m_a R} & (r < R) \\ -\frac{i\pi}{2} \frac{J_1(m_a R) H_0^+(m_a r)}{m_a R} & (r > R) \end{cases}, \quad (3.3)$$

²One way to derive eq. (2.19) from eq. (2.18) is to make use of the identity

$$\vec{\nabla}_y^2 \frac{e^{im_a |\vec{x}-\vec{y}|}}{|\vec{x}-\vec{y}|} = -e^{im_a |\vec{x}-\vec{y}|} \left[4\pi \delta^3(\vec{x}-\vec{y}) + \frac{m_a^2}{|\vec{x}-\vec{y}|} \right]$$

as well as

$$\vec{B}^{\text{ext}}(\vec{x}) = \frac{1}{4\pi} \int d^3y \frac{\vec{\nabla} \times \vec{j}_e(\vec{y})}{|\vec{x}-\vec{y}|},$$

which follows from $\vec{\nabla}^2 \vec{B}^{\text{ext}} = -\vec{\nabla} \times \vec{j}_e$.

where $H_n^+(x)$ is the Hankel function of the first kind of order n . The induced E and B fields resulting from eq. (3.3) are

$$E_{\text{ind}}^z = -g_{a\gamma}a_0B_0e^{-im_at} \begin{cases} 1 - \frac{i\pi}{2}m_aR H_1^+(m_aR)J_0(m_ar) & (r < R) \\ -\frac{i\pi}{2}m_aR J_1(m_aR)H_0^+(m_ar) & (r > R) \end{cases}, \quad (3.4)$$

$$B_{\text{ind}}^\phi = \frac{\pi}{2}g_{a\gamma}a_0B_0e^{-im_at}m_aR \begin{cases} H_1^+(m_aR)J_1(m_ar) & (r < R) \\ J_1(m_aR)H_1^+(m_ar) & (r > R) \end{cases}. \quad (3.5)$$

These results agree with the ones obtained in Ref. [17] by solving the macroscopic equations of motion for the induced EM field for the same configuration. In this case, the boundary conditions that have to be imposed explicitly to solve Maxwell's equations in Ref. [17] are already contained in our approach. They are encoded in the Fourier transform of the static magnetic field.

In the limit of an experiment small compared to the Compton wavelength ($Rm_a \ll 1$) we get

$$E_{\text{ind}}^z \approx \begin{cases} \frac{1}{4}g_{a\gamma}a_0B_0e^{-im_at}(m_aR)^2 \left(1 + i\pi - 2\gamma - 2\log\left(\frac{m_aR}{2}\right) - \left(\frac{r}{R}\right)^2 \right) & (r < R \ll \lambda) \\ \frac{1}{4}g_{a\gamma}a_0B_0e^{-im_at}(m_aR)^2 \left(i\pi - 2\gamma - 2\log\left(\frac{m_ar}{2}\right) \right) & (R < r \ll \lambda) \end{cases}, \quad (3.6)$$

$$B_{\text{ind}}^\phi \approx \begin{cases} \frac{i}{2}g_{a\gamma}a_0B_0e^{-im_at}m_ar & (r < R \ll \lambda) \\ \frac{i}{2}g_{a\gamma}a_0B_0e^{-im_at}m_a \left(\frac{R^2}{r} \right) & (R < r \ll \lambda) \end{cases}, \quad (3.7)$$

with γ being the Euler-Mascheroni constant. Again, the induced magnetic field is suppressed by a factor R/λ and the electric field by a factor $(R/\lambda)^2$ for $R \ll \lambda$. Note that for constant DM energy density, eq. (2.9) implies that $a_0 \propto 1/m_a$. Therefore, in the small experiment limit, the electric field inside the experiment scales as $E_{\text{ind}}^z \propto m_aR^2$, while $B_{\text{ind}}^\phi \propto r$ ($r < R$) and is independent of m_a . In the limit $R \gg \lambda$, the spatial average of the electric field approaches the ‘‘naive’’ solution $E \approx -g_{a\gamma}a_0B_0e^{-im_at}$ and the averaged magnetic field vanishes.

Let us mention that our results agree with Ref. [19] for the magnetic field in the region outside the solenoid, $r > R$, while we disagree for the electric field in the inside region, $r < R$ in the case of small experiment.

4 Discussion and conclusion

To summarize, motivated by recent experimental developments, Refs. [11–13], we have calculated the EM fields induced by dark matter axions in the presence of a static EM field by

using quantum field theory methods. We apply standard techniques to obtain an expression for a transition amplitude describing the interaction of an electron with the background axion and EM fields. The corresponding Feynman diagram is shown in fig. 1. We identify the effective vector potential to which the electron current couples. The internal photon line is described via the Feynman propagator. Indeed, it is the shape of this propagator, together with 4-momentum conservation, which determines the behaviour of the induced field in the three regimes of “small”, “large” or “resonant” configurations. Using the Fourier transform of the external EM field, we obtain an intuitive interpretation in terms of the available momentum modes which the external field can provide, depending on its spatial shape. If the field has a size R large compared to the Compton wavelength λ of the axion, the available momenta are small compared to the axion mass m_a , and can be neglected in the propagator and we obtain the contact-interaction limit adopted, e.g., in Ref. [20]. In the limit of a small experiment ($R \ll \lambda$), the propagator is dominated by the large momenta of the external field, which naturally lead to a suppression of the induced fields by two (one) powers of R/λ for the electric (magnetic) field.

Our results for the induced EM fields agree with the ones from Refs. [17, 18]. However, we find that the results for the induced electric field inside the experiment obtained in Ref. [19] (arXiv v4) do not apply in the case of the “small” experiment, while Ref. [12] assumes they do. The calculations in Ref. [17, 18] are based on classical solutions of Maxwell’s equations. In this traditional approach the appropriate boundary conditions of all involved fields are essential to obtain the correct behaviour in the case of a “small” experiment. Our calculation shows that consistent results can be obtained also by a quantum field theory calculation in terms of the available 4-momentum flow for the virtual photon mediating the interaction.

Let us briefly comment on the resonant case, when the spatial size of the applied field becomes comparable to the axion Compton wavelength. In this case, the detailed shape of the field configuration becomes important. Note that an actual resonant enhancement generally requires additional boundary conditions, beyond the ones encoded in the shape of the applied magnetic field. This can be seen from the explicit calculation for the infinitely long solenoid in section 3: indeed, eqs. (3.4) and (3.5) do not show any resonance as a function of R for fixed m_a . The reason is that, in a configuration as in a resonance cavity or with dielectric layers, additional boundary conditions have to be imposed directly on the photon emitted at the axion-vertex. The appropriate quantum field theory methods to describe such a process have been presented in Ref. [23]. With our ansatz we assume that the induced field is a virtual photon described by the standard Feynman propagator, eq. (2.6), coupling to a fermion current which serves as “detector”.

Finally let us stress, that although we start from a relativistic quantum field theory expression for a transition amplitude, the induced EM field we obtain is classical. While most of the results obtained here are known in the axion literature, our approach offers an alternative derivation and additional physics insights. Employing standard quantum field

theory methods, the calculations presented above provide some clarification in the recent discussion about axion-induced EM fields for experiments exploring the region of small axion masses, below 10^{-7} eV.

Acknowledgments

This project is supported by the European Unions Horizon 2020 research and innovation programme under the Marie Skłodowska-Curie grant agreement No 674896 (Elusives). A.P. acknowledges the support by the DFG-funded Doctoral School KSETA.

A The interaction Hamiltonian

The interaction Hamiltonian can be obtained by the standard canonical formalism, see e.g. Ref. [27]. Let us consider the following Lagrangian density for the photon field

$$\mathcal{L} = -\frac{1}{4}F_{\mu\nu}F^{\mu\nu} - \frac{g_{a\gamma}}{4}aF_{\mu\nu}\tilde{F}^{\mu\nu} - J^\mu A_\mu, \quad (\text{A.1})$$

which is a function of the photon field A_μ and its derivatives. The conjugate momentum is obtained as

$$\pi_\mu \equiv \frac{\delta\mathcal{L}}{\delta\dot{A}^\mu} = -F_{0\mu} - g_{a\gamma}a\tilde{F}_{0\mu}, \quad (\text{A.2})$$

where the dot denotes derivative with respect to time. We find that $\pi_0 \equiv 0$, which implies that A^0 is not a canonical variable and can be eliminated by using equations of motion. The Hamilton density is obtained by a Legendre transform of the Lagrangian density

$$\mathcal{H} = \pi_\mu\dot{A}^\mu - \mathcal{L}, \quad (\text{A.3})$$

where time derivatives of the canonical variables are expressed by their conjugate momenta. Hence we have to replace F_{0i} by π_i using eq. (A.2). Note that \tilde{F}_{0i} only contains the spatial components F^{jk} and therefore no time derivative. From eq. (A.2) we have $\partial^0 A^\mu = -\pi^\mu + \partial^\mu A^0 - g_{a\gamma}a\tilde{F}^{0\mu}$, which gives

$$\mathcal{H} = -\pi_i\pi^i + \pi_i\partial^i A^0 - g_{a\gamma}a\pi_i\tilde{F}^{0i} \quad (\text{A.4})$$

$$+ \frac{1}{2}F_{0i}F^{0i} + \frac{1}{4}F_{ij}F^{ij} + g_{a\gamma}aF_{0i}\tilde{F}^{0i} + J^\mu A_\mu. \quad (\text{A.5})$$

In the last line we have used $F_{\mu\nu}\tilde{F}^{\mu\nu} = 4F_{0i}\tilde{F}^{0i}$. Now we use eq. (A.2) to eliminate F_{0i} in the last line. Keeping terms up to linear order in $g_{a\gamma}$ we find

$$\mathcal{H} = \frac{1}{2}\pi^i\pi^i + \frac{1}{4}F_{ij}F^{ij} - g_{a\gamma}a\pi_i\tilde{F}^{0i} \quad (\text{A.6})$$

$$+ \pi_i\partial^i A^0 + J^\mu A_\mu. \quad (\text{A.7})$$

The second line can be re-written by using the equation of motion following from the Lagrangian eq. (A.1):

$$\partial_\nu F^{\nu\mu} + g_{a\gamma} \partial_\nu (a \tilde{F}^{\nu\mu}) - J^\mu = 0. \quad (\text{A.8})$$

Comparing the zero-component with eq. (A.2) we find $\partial_i \pi^i = J^0$. Hence, the terms in eq. (A.7) can be written as $J^i A_i + \text{total derivative}$, and we have eliminated A^0 from the Hamiltonian.

In summary, the first two terms in eq. (A.6) can be identified with the Hamiltonian of the free electro-magnetic field, while the last term is just the negative of the interaction Lagrangian, eq. (1.1). Hence, we arrive at the result that the interaction Hamiltonian is given by $\mathcal{H}_I = -\mathcal{L}_I$ up to linear order in $g_{a\gamma}$.

B Integrals needed for the infinitely long solenoid calculation

We start from eq. (3.2) and perform the substitution $q \rightarrow k/R$. To evaluate the induced vector potential, we need to solve the integral

$$I(m_a, r, R) \equiv \int_0^\infty dk \frac{1}{m_a^2 R^2 - k^2 + i\epsilon} J_1(k) J_0\left(k \frac{r}{R}\right). \quad (\text{B.1})$$

This integral has a complicated structure but can be reduced to expressions known in the literature. For this purpose, we have to differentiate between the cases $r > R$ and $r < R$:

1. $r > R$: using the Sokhotski-Plemelj theorem, we obtain

$$I(m_a, r, R) = \mathcal{P} \int_0^\infty dk \frac{1}{m_a^2 R^2 - k^2} J_1(k) J_0\left(k \frac{r}{R}\right) + i\pi \text{Res} \left(\frac{1}{m_a^2 R^2 - k^2} J_1(k) J_0\left(k \frac{r}{R}\right) \right), \quad (\text{B.2})$$

where \mathcal{P} denotes the Cauchy principal value. With the help of Ref. [28, p. 463 (57)]

$$\mathcal{P} \int_0^\infty dk \frac{1}{m_a^2 R^2 - k^2} J_1(k) J_0\left(k \frac{r}{R}\right) = \frac{\pi}{2} \frac{J_1(m_a R) Y_0(m_a r)}{m_a R}, \quad (\text{B.3})$$

we get

$$I(m_a, r, R) = -\frac{i\pi}{2} \frac{J_1(m_a R) H_0^+(m_a r)}{m_a R}. \quad (\text{B.4})$$

2. $r < R$: we use integration by parts

$$\begin{aligned} I(m_a, r, R) &= \lim_{\epsilon \rightarrow 0^+} \left[\frac{1}{m_a^2 R^2 - k^2 + i\epsilon} J_0(k) J_0\left(k \frac{r}{R}\right) \right]_0^\infty \\ &+ \lim_{\epsilon \rightarrow 0^+} \int_0^\infty dk \frac{2k}{(m_a^2 R^2 - k^2 + i\epsilon)^2} J_0(k) J_0\left(k \frac{r}{R}\right) \\ &- \lim_{\epsilon \rightarrow 0^+} \frac{r}{R} \int_0^\infty dk \frac{1}{m_a^2 R^2 - k^2 + i\epsilon} J_0(k) J_1\left(k \frac{r}{R}\right), \end{aligned} \quad (\text{B.5})$$

and evaluate the integrals by making use of [29, p. 429 (1)] and [28, p. 462 (44)]

$$\begin{aligned} \lim_{\epsilon \rightarrow 0^+} \int_0^\infty dk \frac{2k}{(m_a^2 R^2 - k^2 + i\epsilon)^2} J_0(k) J_0\left(k \frac{r}{R}\right) \\ = -\frac{i\pi}{2} \frac{H_1^+(m_a R) J_0(m_a r) + \frac{r}{R} H_0^+(m_a R) J_1(m_a r)}{m_a R} \end{aligned} \quad (\text{B.6})$$

$$\begin{aligned} \lim_{\epsilon \rightarrow 0^+} \frac{r}{R} \int_0^\infty dk \frac{1}{m_a^2 R^2 - k^2 + i\epsilon} J_0(k) J_1\left(k \frac{r}{R}\right) \\ = \frac{\pi r}{2 R} \frac{Y_1(m_a R) J_0(m_a r) - i J_0(m_a R) J_1(m_a r)}{m_a R}, \end{aligned} \quad (\text{B.7})$$

to get

$$I(m_a, r, R) = \frac{1}{m_a^2 R^2} - \frac{i\pi}{2} \frac{H_1^+(m_a R) J_0(m_a r)}{m_a R}. \quad (\text{B.8})$$

Equation (3.3) follows from eq. (B.4) and eq. (B.8).

References

- [1] S. Weinberg, *A New Light Boson?*, *Phys. Rev. Lett.* **40** (1978) 223–226.
- [2] F. Wilczek, *Problem of Strong P and T Invariance in the Presence of Instantons*, *Phys. Rev. Lett.* **40** (1978) 279–282.
- [3] P. Sikivie, *Experimental Tests of the Invisible Axion*, *Phys. Rev. Lett.* **51** (1983) 1415–1417.
- [4] I. G. Irastorza and J. Redondo, *New Experimental Approaches in the Search for Axion-Like Particles*, *Prog. Part. Nucl. Phys.* **102** (2018) 89–159, [[1801.08127](#)].
- [5] ADMX, N. Du et al., *A Search for Invisible Axion Dark Matter with the Axion Dark Matter Experiment*, *Phys. Rev. Lett.* **120** (2018), no. 15 151301, [[1804.05750](#)].
- [6] HAYSTAC, L. Zhong et al., *Results from Phase 1 of the Haystac Microwave Cavity Axion Experiment*, *Phys. Rev.* **D97** (2018), no. 9 092001, [[1803.03690](#)].
- [7] C. Woohyun, *CULTASK, the Coldest Axion Experiment at CAPP/IBS in Korea*, *PoS ICHEP2016* (2016) 197.
- [8] MADMAX Working Group, B. Majorovits and J. Redondo, *MADMAX: A new Dark Matter Axion Search using a Dielectric Haloscope*, in *Proceedings, 12th Patras Workshop on Axions, WIMPs and WISPs (PATRAS 2016): Jeju Island, South Korea, June 20-24, 2016*, pp. 94–97, 2017. [[1611.04549](#)].
- [9] P. Sikivie, N. Sullivan, and D. B. Tanner, *Proposal for Axion Dark Matter Detection Using an Lc Circuit*, *Phys. Rev. Lett.* **112** (2014), no. 13 131301, [[1310.8545](#)].

- [10] Y. Kahn, B. R. Safdi, and J. Thaler, *Broadband and Resonant Approaches to Axion Dark Matter Detection*, *Phys. Rev. Lett.* **117** (2016), no. 14 141801, [[1602.01086](#)].
- [11] J. L. Ouellet et al., *First Results from ABRACADABRA-10 cm: A Search for Sub- μ eV Axion Dark Matter*, [1810.12257](#).
- [12] B. T. McAllister, M. Goryachev, J. Bourhill, E. N. Ivanov, and M. E. Tobar, *Broadband Axion Dark Matter Haloscopes via Electric Sensing*, [1803.07755](#).
- [13] M. Silva-Feaver et al., *Design Overview of Dm Radio Pathfinder Experiment*, *IEEE Trans. Appl. Supercond.* **27** (2017), no. 4 1400204, [[1610.09344](#)].
- [14] C. Gatti et al., *The Klash Proposal: Status and Perspectives*, in *14th Patras Workshop on Axions, WIMPs and WISPs (AXION-WIMP 2018) (PATRAS 2018) Hamburg, Germany, June 18-22, 2018*, 2018. [1811.06754](#).
- [15] R. D. Peccei and H. R. Quinn, *Constraints Imposed by CP Conservation in the Presence of Instantons*, *Phys. Rev.* **D16** (1977) 1791–1797.
- [16] R. D. Peccei and H. R. Quinn, *CP Conservation in the Presence of Instantons*, *Phys. Rev. Lett.* **38** (1977) 1440–1443.
- [17] J. Ouellet and Z. Bogorad, *Solutions to Axion Electrodynamics in Various Geometries*, [1809.10709](#).
- [18] Y. Kim, D. Kim, J. Jung, J. Kim, Y. C. Shin, et al., *Effective Approximation of Electromagnetism for Axion Haloscope Searches*, [1810.02459](#).
- [19] M. E. Tobar, B. T. McAllister, and M. Goryachev, *Modified Axion Electrodynamics Through Oscillating Vacuum Polarization and Magnetization and Low Mass Detection Using Electric Sensing*, . [1809.01654v4](#).
- [20] J. Hong and J. E. Kim, *A New Method for Detectability of Oscillating Theta*, *Phys. Lett.* **B265** (1991) 197–200.
- [21] C. T. Hill, *Axion Induced Oscillating Electric Dipole Moments*, *Phys. Rev.* **D91** (2015), no. 11 111702, [[1504.01295](#)].
- [22] C. T. Hill, *Axion Induced Oscillating Electric Dipole Moment of the Electron*, *Phys. Rev.* **D93** (2016), no. 2 025007, [[1508.04083](#)].
- [23] A. N. Ioannisian, N. Kazarian, A. J. Millar, and G. G. Raffelt, *Axion-Photon Conversion Caused by Dielectric Interfaces: Quantum Field Calculation*, *JCAP* **1709** (2017), no. 09 005, [[1707.00701](#)].
- [24] S. Knirck, A. J. Millar, C. A. J. O’Hare, J. Redondo, and F. D. Steffen, *Directional Axion Detection*, *JCAP* **1811** (2018), no. 11 051, [[1806.05927](#)].
- [25] J. W. Foster, N. L. Rodd, and B. R. Safdi, *Revealing the Dark Matter Halo with Axion Direct Detection*, *Phys. Rev.* **D97** (2018), no. 12 123006, [[1711.10489](#)].
- [26] J. D. Jackson, *Classical electrodynamics*. Wiley, 3rd ed., 1999.

- [27] S. Weinberg, *The Quantum Theory of Fields, Volume 1: Foundations*. Cambridge University Press, 2005.
- [28] Q.-G. Lin, *Infinite integrals involving bessel functions by an improved approach of contour integration and the residue theorem*, *The Ramanujan Journal* **35** (2014) 443–466.
- [29] G. Watson, *A Treatise on the Theory of Bessel Functions*. Cambridge Mathematical Library. Cambridge University Press, 1995.